Climate Dynamics (2025) 63:19
https://doi.org/10.1007/s00382-024-07490-x

ORIGINAL ARTICLE

Diagnostics of the solar activity influence on the global atmospheric circulation in the thermosphere and MLT area: wave—mean flow interaction effects

Andrey V. Koval[1,2] · Kseniia A. Didenko[1,3] · Tatiana S. Ermakova[1,2] · Nikolai M. Gavrilov[1] · Anastasia G. Golovko[1]

Received: 10 June 2024 / Accepted: 6 November 2024
© The Author(s), under exclusive licence to Springer-Verlag GmbH Germany, part of Springer Nature 2024

Abstract
Using the mechanistic nonlinear Middle and Upper Atmosphere Model "MUAM", the influence of solar activity (SA) on the dynamics of the mesosphere and lower thermosphere (MLT) area and thermosphere is considered from the point of view of the interaction of the mean atmospheric circulation with planetary waves (PWs) and tides. This interaction is analyzed within the Transformed Eulerian Mean approach and interpreted by calculating the Eliassen-Palm flux and the residual mean meridional circulation (RMC). Two ensembles of hydrodynamic fields for January, consisting of 16 model runs, corresponding to high and low SA, are considered. It is shown that with increasing solar influence at high SA, wave activity decreases in the layer between 100 and 170 km, while in higher layers an increase in wave activity occurs. This behavior may be explained by a number of factors contributing to the weakening PWs and increasing tides. Among them are an increase in temperature, viscosity and vertical temperature gradients at high SA. At the same time, the dominant role of tides in the change of wave activity in the thermosphere is detected, while the PW amplitudes and their EP fluxes have significantly smaller values. An analysis of the thermosphere dynamic regime at increasing SA shows that the strengthening of the RMC above 200 km is determined by changes in the mean Eulerian circulation. Modifications of the dynamic and temperature regime of the thermosphere caused by SA lead to changes in RMC in the MLT of up to 10%. The main role in these changes is played by increasing reflection of PWs above 100 km altitude due to increasing vertical temperature gradients at high SA.

Keywords General circulation · Numerical modeling · Solar activity · Thermosphere · Planetary waves

1 Introduction

Planetary waves generated in the troposphere due to orographic inhomogeneities, barotropic/baroclinic instability or caused by sea-land contrasts, propagate into the upper atmosphere and, due to the exchange of momentum and energy with atmospheric circulation, have a significant impact on the global atmospheric circulation. In particular, in appliance with the "Downward Control Principle" first proposed by (Haynes et al. 1991), wave disturbances are the most important driving mechanism influencing the meridional circulation. Therefore, the study of meridional transport in all atmospheric layers is inextricably linked with the consideration of atmospheric waves, both macroscale planetary and mesoscale gravity waves (PWs and GWs, respectively). At the same time, along with the rapid development of numerical modeling of the atmospheric general circulation, interest in a better understanding of the temperature and dynamic effects caused by wave movements, such as PWs, in various layers of the atmosphere is growing. Much attention is also paid to the mechanism of global transport of trace gases between different atmospheric layers (see, e.g., Fishman and Crutzen 1978), provided by the Brewer-Dobson meridional circulation (BDC) (Dobson 1956; Brewer 1949). The BDC carries out global mass transfer, including upwelling of tropospheric air at low latitudes, poleward mass transport and downwelling at the middle and high latitudes

✉ Andrey V. Koval
a.v.koval@spbu.ru

[1] Department of Atmospheric Physics, St. Petersburg University, St. Petersburg, Russia

[2] Department of Meteorological Forecasts, Russian State Hydrometeorological University, St. Petersburg, Russia

[3] Pushkov Institute of Terrestrial Magnetism, Ionosphere, and Radio Wave Propagation (IZMIRAN), Russian Academy of Sciences, Troitsk, Moscow, Russia

Published online: 02 December 2024

(Butchart et al. 2014). At mesosphere altitudes and above, the global meridional circulation represents the summer-to-winter transfer of mass from one hemisphere to the other. (see, e.g., Holton et al. 1995) with narrow winter-to-summer meridional branch in the lower thermosphere (e.g. Qian et al. 2017; Lilienthal et al. 2020; Wang et al. 2022). The study of meridional circulation within the Transformed Eulerian Mean (TEM) framework, developed by Andrews and McIntyre (1976), has become widely-used for treating global atmospheric dynamics. The residual meridional circulation (RMC) calculated within this framework is a combination of advective and eddy mean meridional transport (e.g., Shepherd 2007). Calculation of circulation within the TEM approach is used the study and forecasting of possible changes in the transport of atmospheric tracers (e.g., Gerber et al. 2012; Teng et al. 2021; Eyring et al. 2005; Laskar et al. 2019; Vargin et al. 2023).

The features of the spatial and temporal structures of PWs, and consequently the circulation determined by them, depend on variations in direct solar irradiance, depending on solar activity (SA) (see e.g., Balogh et al. 2014). In particular, changes in incoming solar energy affect the temperature profile and circulation flows, modifying the PW waveguides and hence, the conditions for wave propagation into the middle and upper layers of the atmosphere (Arnold and Robinson 1998, 2000; Geller and Alpert 1980). For example, Arnold and Robinson (2000), based on modeling results, indicated that inclusion of the upper atmosphere can lead to a significant enhancement of the influence of SA on the middle atmosphere dynamics through radiative/dynamical coupling of planetary waves. In turn, changes in PW patterns due to momentum exchange affect the zonal circulation, and wave dissipation also contributes to the acceleration of meridional circulation and heating of atmospheric layers. Hence, there is a complex cause-and-effect relationship between wave disturbances and mean flow, modulated by SA. Several early studies, for example, pointed to a dependence of the stratospheric polar vortex on quasi-biennial oscillation (QBO), which could be modulated by SA (Labitzke 1987; Naito and Hirota 1997; Cai et al. 2022). The mechanism of signal transmission from disturbances in the stratosphere, related to sudden stratospheric warmings, to the ionosphere through vertical wave interaction was investigated recently using the Entire Atmosphere GLobal model (EAGLE) by Klimenko et al. (2019). Significant progress in studying the effects of solar radiation on atmospheric dynamics has been achieved thanks to the ROSMIC initiative (Role Of the Sun and the Middle atmosphere/thermosphere/ionosphere In Climate, Ward et al. 2021). In the course of the ROSMIC project, new observation methods, data analysis and modeling methods were developed. While the new data has clarified some aspects of the Earth's connection to the thermosphere/ionosphere, it has also raised many new questions. In particular, much attention in the project was paid to GWs: their characteristics of propagation and dissipation depending on solar irradiance (e.g., Laskar et al. 2015; Liu 2016; Mandal et al. 2020). When studying vertical interactions in the atmosphere, special attention should be paid also to PWs, both propagating into the thermosphere from below and those generated in situ (e.g., Arnold and Robinson 2000; Forbes et al. 2018, 2020; Takahashi et al. 2007).

In the recent investigation, Teng et al. (2021) performed numerical experiments to study the influence of SA on the atmospheric dynamic processes up to 500 km using the Whole Atmosphere Community Climate Model with thermosphere and ionosphere eXtension with specified dynamics (SD-WACCM-X). They discussed that SA has a substantial impact on the circulation of the upper atmosphere, and namely, the strengthening of SA can enhance atmospheric flows intensity. Using another version of this model (WACCM-X), Sun et al. (2022) found correlations between solar tides and SA in the mesosphere and lower thermosphere (MLT) area. However the correlations may vary in time and space. Kuroda et al. (2007) noted an increase in the stratosphere-troposphere interaction under high SA conditions. A detailed analysis of the reaction of the meridional circulation to SA in the stratosphere and MLT area during solstices was carried out by Karlsson and Kuilman (2018). In particular, they demonstrated the interaction of direct solar heating with meridional circulation tending to adiabatic cooling of the summer mesosphere, and described the detailed chain of events that determines this mechanism. Krivolutsky et al. (2015) used the mechanistic general circulation model "ARM" to study the influence of SA changes on the zonal wind and temperature in the stratosphere and noted the essential role of PWs in the implementation of the SA impact on climate due to the vertical coupling of the atmospheric layers.

An important factor influencing global circulation is downward reflection of PW activity at various levels. Typically, PW reflection is considered at stratosphere altitudes (e.g., Kodera et al. 2008; Perlwitz and Harnik 2004; Nath et al. 2014; Lu et al. 2017). However, as shown by Koval et al. (2019b), the reason for the PW reflection may be significant temperature and wind speed gradients in the lower thermosphere, caused by direct solar influence in the thermosphere, which increases at high SA. These gradients are capable of changing wave activity fluxes and waveguides and hence the proportion of upward transmitted and reflected wave energy.

In this study, we continue the series of studies dedicated to modeling the response of global atmospheric circulation to dynamic and temperature variations in the thermosphere caused by SA changes within the 11-year solar cyclicity. In particular, the impact of changes in SA in the thermosphere

on the structures of stationary PWs, wave reflection in the lower thermosphere and associated changes in zonal circulation in the middle atmosphere are considered by Koval et al. (2018b, 2019b). Changes in waveguides and amplitudes of atmospheric normal modes and corresponding planetary wave-type oscillations in the thermosphere (in geopotential, temperature and horizontal wind fields) are discussed in (Koval et al. 2018a). In a study by Koval et al. (2022a), we also compared the simulated with the MUAM spectra of tides and PWs with observational data of variations in the critical frequency in the ionosphere using ionosonde observations in St. Petersburg. This work is aimed to consider for the first time interaction of atmospheric circulation with PWs and tides to analyze the relationship between SA changes and thermal/dynamical regimes of the MLT area and thermosphere. This wave-mean flow interaction is considered within the TEM approach and interpreted by calculating the RMC vertical and meridional components as well as Eliassen-Palm (EP) flux and EP flux divergence. The RMC components calculated in this way represent a combination of the Brewer-Dobson circulation in the stratosphere and the pole-to-pole circulation in the MLT area and above.

The paper is structured as follows: Sect. 2 describes the features of accounting for SA in the MUAM model, presents a brief description of the model experiment and methods for interpreting data. Section 3 with the results of the study is divided into two parts, dedicated to the thermosphere and the MLT region, respectively. Final remarks and general conclusions are presented in Sect. 4.

2 Methods and approaches

As in previous works dedicated to studying the sensitivity of large-scale wave processes to changes in SA (Koval et al. 2018a,b, 2019b, 2022a), the mechanistic Middle and Upper Atmosphere Model "MUAM" (Pogoreltsev et al. 2007) is used in this study. This nonlinear model is based on solving the primitive equation set of hydrodynamics in spherical coordinates, with a horizontal grid of 36 by 64 cells and 56 vertical cells from the surface to 300 km along a log-isobaric coordinate. We consider solar radiation flux *F10.7* as the main indicator of SA. The *F10.7* flux undergoes variations associated to the 11-year solar cycle (e.g., Balogh et al. 2014). Having processed *F10.7* variations over six solar cycles using data from the Royal Observatory of Belgium (ROB), we selected *F10.7* = *70, 130, 220* sfu (1 sfu = 10–22 W/(m^{2}Hz)) as characteristics of low, medium and high SA, respectively. In order to study the response of different SA occurring only in the thermosphere, including the transfer of this effect to the middle atmosphere, SA changes (low and high SA) were included in the MUAM radiation block above 100 km. Below this level all numerical calculations involved identical values of *F10.7*, characterizing medium SA level. Solar fluxes and absorption coefficients for each ultraviolet spectral range in thermosphere were calculated using the model proposed by Richards et al. (1994). In addition, the impact of charged particles on the neutral gas movement in the ionosphere is calculated in the MUAM. For this purpose, ionospheric conductivities were calculated for the mentioned above low and high SA levels using the semi-empirical International Reference Ionosphere model Extended to Plasmasphere (IRI-Plas, Gulyaeva et al. 2002). These ionospheric conductivities were implemented in MUAM. Details of the calculation of ionospheric conductivities and their inclusion in the MUAM are presented in (Koval et al. 2018b). This research scenario was chosen in order to take into account the direct impact of solar radiation in the thermosphere only (see, e.g., Kodera and Kuroda 2002) and to investigate patterns in the dynamic connection between upper and middle atmosphere by means of PW interactions. In this case we do not simulate changes in direct solar influence on the middle atmosphere.

Sources of stationary PWs in MUAM are determined at the lower boundary as horizontal inhomogeneities of geopotential heights, averaged for 2005–2014 according to Japanese 55-year Reanalysis of meteorological information (JRA-55, Kobayashi et al. 2015). Sources of atmospheric normal modes with periods of 2–16 days are set using respective terms in the MUAM equation of the heat balance, involving Hough functions calculated as it was proposed by Schwartztrauber and Kasahara (1985). This approach makes it possible to reproduce in the MUAM spatiotemporal PW structures similar to ones observed in the real atmosphere. Koval et al. (2019b) compared the simulated structures of the stationary PWs with satellite observation data (Forbes et al. 2002; Xiao et al. 2009). In particular, the structures of stationary PW with zonal wavenumber 1 up to altitudes of 120 km were compared with TIMED/SABER temperature measurements (Mukhtarov et al. 2010). The PWs amplitudes in the MUAM were found to correspond to the observational data on temperature variations.

To take into account the dynamic and thermal effects of mesoscale gravity waves (GWs) that are not resolved on the MUAM model grid, parameterizations are used. For internal non-orographic GWs, depending on the GW phase velocities c, a spectral parameterization developed by Yigit and Medvedev (2009) is used ($c = 30–125$ m/s) and the Lindzen parameterization scheme (Lindzen 1981) ($c = 5–30$ m/s). Stationary orographic GWs are parameterized by the method proposed by Gavrilov and Koval (2013). Further information about parameterizations is presented in Lilienthal et al. (2018), Geißler et al. (2020).

Detailed information of the numerical experiment and calculation of statistical significance based on 16-member ensembles of model simulations is presented by Koval et al. (2019b).

The calculation of each model run begins with a windless state using the global mean temperature distribution for January from the JRA-55. Daily-mean heating rates are involved in the MUAM during the first 120–135 model days. After that, daily changes in solar heating are taken into account and sources of atmospheric normal modes are turned on. Seasonal changes in the solar zenith angle are taken into account after 330th model day, hence, during days 330–390 the simulation of the general circulation for January–February is performed. Changing the model day of the onset of the sources of normal modes and daily changes in solar heating between model days of 120 and 135 control phases of vacillations of the mean horizontal wind and PWs (Holton and Mass 1976; Pogoreltsev 2007) in the model. Averaging over an ensemble of 16 model runs is interpreted as the mean "climatic" distribution of hydrodynamic fields, as far as variability of the monthly-mean PW amplitudes, temperature and mean flow intensity between different model runs is interpreted as interannual (Pogoreltsev 2007).

The residual meridional circulation is considered in terms of the Transformed Eulerian Mean circulation (TEM, Andrews and McIntyre 1976). The RMC is calculated using conventional formulas (e.gAndrews et al. 1987; Holton 2004):

$$\overline{v^*} = \overline{v} - \rho^{-1}\frac{\partial}{\partial z}\left(\rho\frac{\overline{v'\theta'}}{\frac{\partial\overline{\theta}}{\partial z}}\right), \tag{1}$$

$$\overline{w^*} = \overline{w} + \frac{1}{a\cos\varphi}\frac{\partial}{\partial\varphi}\left(\frac{\cos\varphi\overline{v'\theta'}}{\frac{\partial\overline{\theta}}{\partial z}}\right), \tag{2}$$

where the primes indicate wave disturbances resolved on the model grid; the overbars denote zonal-mean quantities; v and w—meridional and vertical wind; θ—potential temperature; z—vertical coordinate; ρ—density; φ—latitude; a is the Earth's radius. The dependence of the RMC on wave disturbances makes the TEM approach a convenient method for analyzing and interpreting nonstationary interactions of PWs with the mean circulation flows (Bal et al. 2018; Koval et al. 2023).

An important characteristic that allows one to analyze the PW—mean flow interaction is the Eliassen-Palm flux vector (EP flux), $\boldsymbol{F} = \left(F^{(\varphi)}, F^{(z)}\right)$ (Jucker 2021):

$$F^{(\varphi)} = \cos\varphi\left(\overline{u}_z\frac{\overline{v'\theta'}}{\overline{\theta}_z} - \overline{u'v'}\right), \tag{3}$$

$$F^{(z)} = \cos\varphi\left(\left(f - \frac{(\overline{u}\cos\varphi)_\varphi}{a\cos\varphi}\right)\frac{\overline{v'\theta'}}{\overline{\theta}_z} - \overline{w'u'}\right), \tag{4}$$

where subscripts denote partial derivatives; f—Coriolis parameter; u—zonal wind. Note that Eqs. (3) and (4) are written within the quasi-geostrophic approximation and divided by ρ and a. In this form they are presented in the figures below. It is believed that the main contribution to the vertical wave activity flux is made by the eddy heat flux (e.g., Kodera et al. 2008): the upward direction of the EP flux corresponds to the poleward directed heat flux. Eastward/westward acceleration of the zonal flow due to the exchange of momentum with the PW is expressed in the positive/negative EP flux divergence.

3 Results and discussion

To study the influence of SA on the large-scale dynamical structure of the thermosphere and the MLT area, we consider the fields of atmospheric parameters simulated in MUAM for January at high and low SA, obtained by processing 16-member ensembles of model simulations. Our comparative analysis (Koval et al. 2018a) showed that the temperature, density and pressure fields simulated with the MUAM are consistent with those calculated with the empirical atmospheric model NRLMSISE-00 (Picone et al. 2002), using the same *F10.7* values and same time interval. In addition, the zonal/meridional wind and temperature fields in the middle atmosphere were compared with the reanalysis: MERRA-2 (Modern-Era Retrospective analysis for Research and Applications, Version 2) data in (Koval et al. 2022b); JRA-55 data in (Koval et al. 2019a); ERA-Interim data in (Zorkaltseva et al. 2020).

3.1 Thermospheric response to SA variability

3.1.1 Wave activity

Figure 1 shows the latitude-height distributions of thermospheric EP fluxes (a), zonal-mean temperature and RMC components (b) and zonal wind (c) for January at low SA (top panels), as well as changes in these parameters under high SA conditions. Bottom panels of Fig. 1 show that SA variations in the thermosphere can make a substantial contribution to the distributions of all dynamic parameters. At the same time, large increments provide statistical significance of more than 95% according to the t-test at all heights, in areas where these increments are different from zero.

Figure 1a2 demonstrates that wave activity decreases in the layer between 100 and 170 km under increasing solar influence at high SA. In particular, the increments of the vertical EP flux component, shown by color coding, are negative. Accordingly, the upward propagation of wave activity at high SA is weakened or even turns downward, indicating conditions favorable for the PW reflection. Such

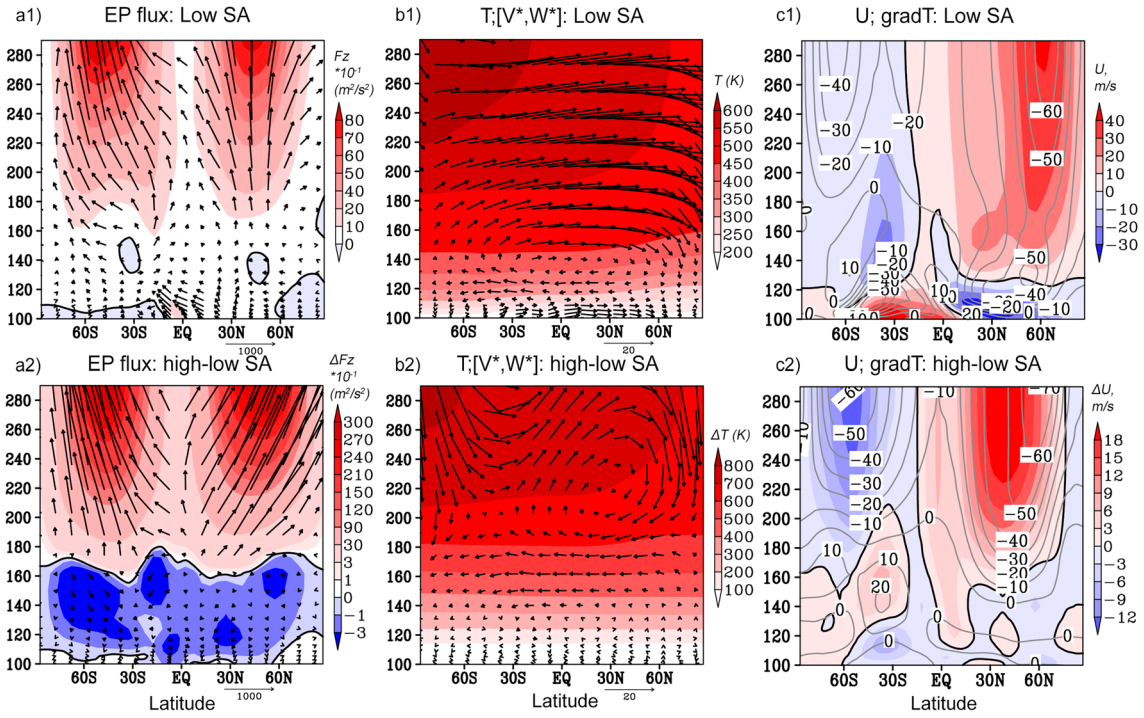

Fig. 1 Latitude-height distributions: **a**—EP flux (m^2/s^2, arrows) and its vertical component (color coded); **b**—zonal-mean temperature (K, color coded) and RMC components (m/s, arrows); **c**—zonal wind (m/s, color coded) and meridional thermal gradient (K/deg, contours). The top row corresponds to low SA, the bottom row shows the difference in the indicated parameters between high and low SA. The vertical components of the RMC and EP flux are multiplied by 200

reflected PWs have a further impact on the dynamics of the underlying layers, which will be discussed in the next subsection. Similar PW reflection effects caused by changes in UV forcing (and hence changes in the background temperature profile) in the upper stratosphere have also been found previously (e.g., Lu et al. 2017). In the studies by Koval et al. (2018a, 2019b) this effect was noted in the lower thermosphere and it was demonstrated how an increase in PW reflection leads to a change in the proportion of reflected and upward penetrated wave activity. Above the level of 160–180 km in Fig. 1a2, we see the wave activity increase: the arrows of EP flux increments are aligned with the flux arrows in Fig. 1a1 at all latitudes, while the flux at high SA can be more than twice as large as the flux at low SA. According to the formulas (3) and (4), EP flux is determined by temperature and velocity disturbances (deviations from the zonal-mean values). The sources of such disturbances, resolved on the MUAM spatial grid, include planetary waves and tides.

To explain the nature of changes in EP fluxes in Fig. 1a2, which are multidirectional at different layers of the thermosphere, we analyzed PWs and tides for January, which were calculated using the longitude-time Fourier transform of geopotential height fields followed by a least square fitting. To improve statistical significance, we averaged PW and tide amplitudes calculated for the 15-day intervals (i.e. two intervals for January) for each model run within the ensemble as it was proposed by Koval et al. (2019b). The analysis showed that the amplitudes of stationary PWs and migrating tides in the thermosphere are maximum compared to other PW modes and tides (see also Koval et al. 2018a, 2019b). To assess the interaction of the PWs and tides with the mean flow, the EP fluxes were calculated for each of the considered PW and tide modes. Figure 2 shows the calculated amplitudes and EP fluxes for stationary PWs with zonal wavenumbers 1 and 2 and migrating diurnal and semidiurnal tides. The possibility to reproduce correctly PW structures with the MUAM was discussed in earlier studies, where PW amplitudes were compared to other simulations and remote sensing data, including meteor radars and ionosondes (Koval et al. 2018a, 2019b, 2022a, 2023 and references therein). As previously discussed by Koval et al. (2019b), PWs in the thermosphere increase with height (Fig. 2a1 and b1), however, at high SA their values are much smaller, as demonstrated by the amplitude differences in Fig. 2a2 and b2. This effect can be explained as follows. At high SA, in the lower thermosphere, the vertical temperature gradient increases significantly, which can be seen in Fig. 1b1 and b2. This is accompanied by a strong increase in the buoyancy frequency N. Due to the PW dispersion relation, an increase in N leads

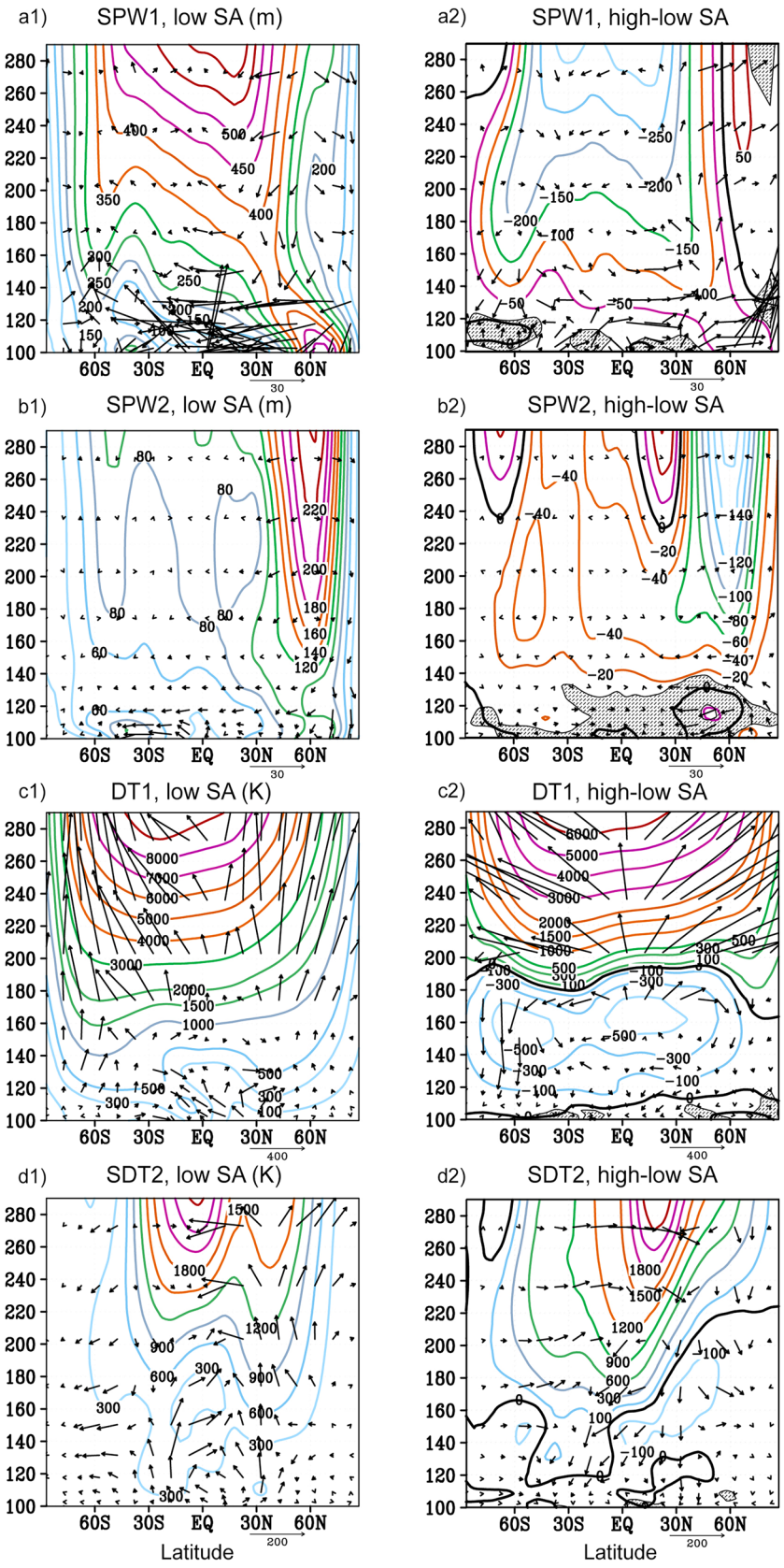

Fig. 2 Amplitudes of variations of geopotential height due to stationary PWs with zonal wavenumbers 1 and 2 and thermal migrating diurnal and semidiurnal tides (gp.m., **a**–**d**, respectively) in the altitudes between 100 and 290 km for January. Arrows show EP fluxes (m^2s^{-2}, vertical component is multiplied by 200). The left column corresponds to low SA, the right column shows the difference in the indicated parameters between the high and low SA. Hatched areas indicate statistically insignificant amplitude increments (at 95%)

to an increase in the vertical wavenumber m (e.g., Andrews et al. 1987). The wave activity flux $\boldsymbol{F}_a = \boldsymbol{c}_g A$, depends on the group velocity $\boldsymbol{c}_g$ and the wave activity density A. Decreasing in the vertical component of the group velocity occurs, as $c_{gz} \sim m^{-1}$. As a result, this leads to a weakening of the vertical wave activity flux at high SA due to an increase in the vertical temperature gradient. Another explanation is the reduction of the atmospheric refractive index and the narrowing of the waveguide for the PW, as discussed in (Koval et al. 2019b). These factors, in addition to ion drag and thermal conductivity, which is proportional to temperature, make it difficult for PWs to penetrate into the thermosphere to greater heights at high SA.

It should be noted that the direct passage of most PW modes into the thermosphere is hampered by the critical layers in the lower thermosphere. The exceptions are eastward travelling fast PWs (e.g., Takahashi et al. 2007) and tides (e.g., Sun et al. 2022). However, there are many examples of observation of coexistence of PWs with similar periods in the lower, middle and upper layers of the atmosphere. Laštovicka (2006) suggested that PWs can propagate from the middle atmosphere above 130–140 km indirectly, through secondary excitation of PWs, for example, due to modulation of PWs by tides (see also Yamazaki and Richmond 2013), or by means of vertical drift of plasma (Liu and Richmond 2013). Being the nonlinear numerical model, MUAM perfectly reproduces secondary planetary waves generation through nonlinear interactions. This effect we demonstrated recently using the example of the generation of a 16-day PW during the interaction of 4- and 5-day PWs in the upper atmosphere (Didenko et al. 2024).

The nature of the propagation of migrating tides with a frequency that is a multiple of the day is completely different. The mechanisms discussed above for PWs also contribute to the weakening of tidal amplitudes. This is clearly seen at altitude range of 100–180 km in Fig. 2c2, d2. However, a greater contribution to the development of these oscillations is made by the increased absorption of direct EUV radiation, which increases at high SA. This effect dominates above 170–180 km, and tidal amplitudes at higher altitudes at maximum SA increase faster than at low SA. A similar negative correlation between the amplitude of the diurnal tide (albeit in the zonal wind field) at altitudes of 100–140 km and a positive one at higher altitudes was recently discussed by Sun et al. (2022). The effect of tidal weakening at high SA at altitudes of about 120 km, similar to what we observed, but using the example of a diurnal non-migrating tide, was discussed in the study of Oberheide et al. (2015). Our calculations of the diurnal tide amplitudes based on the DPS-4 ionosonde data, when analyzing the critical frequency of the F2 layer using the method described in Koval et al. (2022a), showed an increase in tide at an altitude of about 200 km. The trends in the change of the semidiurnal tide in Fig. 2b2 are generally similar to the changes in the diurnal tide in Fig. 2a2, with the exception of the low-latitude region below 160 km, where a noticeable shift in the maximum tide to the Southern Hemisphere is noticeable. The EP fluxes in Fig. 2 demonstrate the direction of propagation of wave activity for the corresponding PW and tidal modes, as well as changes in this propagation at high SA. In general, it is clear that the strengthening of tides at high SA below/above ~ 180 km is accompanied by decrease/increase in ascending EP fluxes in Fig. 2c2 and d2, while the weakening of PWs in Fig. 2a2 and b2 is accompanied mainly by a weakening of the EP fluxes. At the same time, the values of the amplitudes and EP fluxes of tides significantly exceed the corresponding PW indicators, which shows the dominant role of the former in changes in the global dynamics of the thermosphere, demonstrated in Fig. 1.

3.1.2 The RMC

Arrows in Fig. 1b1 and b2 show the components of the RMC under low SA conditions and their changes at high SA, respectively. The demonstrated strengthening of the meridional RMC component above 200 km has been discussed, e.g., by Teng et al. (2021). However, the most interesting are significant fluctuations in the vertical RMC component, resulting in the RMC increments directed downward at high and middle latitudes and upward in the low-latitude region. Figures 3a1 and 3b1 demonstrate, respectively, the Eulerian mean meridional circulation and the eddy meridional circulation, induced by PWs and tides resolved on the MUAM spatial grid (the terms presented on the right-hand side of Eqs. 1 and 2). The structure of the simulated meridional circulation in the thermosphere (Fig. 3a1) is typical for boreal winter conditions: above about 130 km, the meridional summer-to-winter transport predominates, which is mainly exerted by the pressure meridional gradient caused by latitudinally asymmetric solar heating (Fuller-Rowell 1998). To generate meridional motion by a pressure gradient, it is necessary that the Coriolis force be compensated in extratropical regions by zonal momentum forcing. And these conditions are met in the thermosphere, where the zonal-mean zonal wind is directed predominantly to the west in the summer and to the east in the winter hemisphere (Fig. 1c1). In the underlying layers (between 100 and 130 km) the meridional circulation turns backwards: from the winter to the summer hemisphere. This effect was discussed in detail by Wang et al. (2022): they showed that the main reason for such movements is the dissipation of GWs with high phase velocities propagating from below and unfiltered by zonal wind gradients in the mesosphere. Such GWs, propagating into the lower thermosphere (up to altitudes approximately 100–130 km) and dissipating there due to an increase in molecular diffusion and ion drag, can transmit momentum to

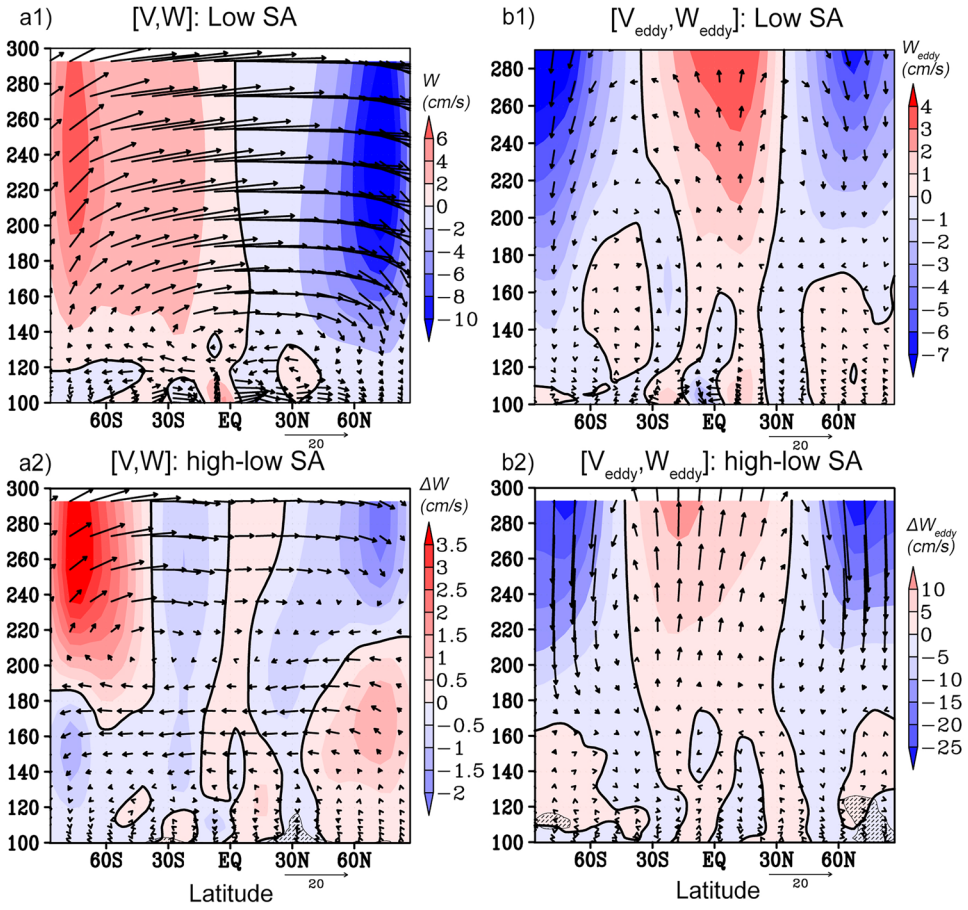

Fig. 3 Latitude-height distributions: the mean Eulerian meridional circulation (**a**) and the eddy component of the RMC (**b**) (the terms presented on the right side of Eqs. 1 and 2) at low SA (top panels) and the corresponding increments (bottom panels). Arrows show meridional and vertical (multiplied by 200) components. The vertical component is also shown by color coding. Hatched areas indicate statistically insignificant data (for both, meridional and vertical components)

the mean flow. This accumulation of momentum in the lower thermosphere contributes to reversal of zonal jet streams in the 100–130 km layer shown in Fig. 1c1.

Figures 3a2 and b2 show the increments of Eulerian mean and eddy meridional circulation due to an increase in SA. It can be seen that the strengthening of the meridional component of the RMC in Fig. 1b2 above 200 km is determined by a change in the Eulerian circulation, due to an increase in the direct effect of the EUV and, consequently, pressure gradient caused by solar heating. Below 200 km in Fig. 3a2 there is a weakening of meridional transport at high SA, and an increase in circulation directed from the winter to the summer hemisphere. This effect can be associated with two mechanisms: (1) a general weakening of the wave activity of the PWs and tides resolved on the model grid, shown in Fig. 1a2 and (2) increased GW dissipation due to changes in background density and temperature, as discussed by Laskar et al. (2015). In Fig. 3a2 and b2, the statistical significance according to the Student's t-test remains greater than 95% even in areas where the increments are close to zero. This is explained by the large sample (daily data are used, a total of 31 time points * 16 model runs in the ensemble = 496 sample size), as well as the weak variability of the studied fields in these areas. This can be interpreted as follows: at the significance level of 95%, the changes in the studied parameters are zero.

The sensitivity of the vertical RMC component to SA variations at altitudes greater than 200 km is determined mainly by the eddy RMC part, which increments are shown in Fig. 3b2. Ascending eddy flows are localized in the latitudinal band 30° S–30° N, along the trajectory of the diurnal thermal tide, and are compensated by downward flows in the subpolar and middle latitudes.

Increased solar influence also contributes to an increase in the speed of zonal flow, shown in Fig. 1c2. Despite the growth in braking factors, such as ion drag and viscosity with increasing SA, the strengthening in thermal gradients, according to the equation for the thermal wind (e.g., Cai et al. 2022), increases the vertical shear of the zonal wind: eastward in the Northern Hemisphere and westward in the Southern one.

3.2 The influence of SA changes on the MLT area

As it is known, due to the quasi-exponential decrease in pressure with height, any disturbances occurring in the thermosphere directly (e.g., due to solar influence variations) spreading downwards, quickly fade and cannot significantly

affect the underlying layers. And in our experiment, the change in SA is set above 100 km, and cannot affect the MLT area directly. However, such changes were documented by Koval et al. (2019b). It was suggested that changes in wind shears and temperature gradients in lower layers of the thermosphere can contribute to the reflection of the PW propagating from below back to the lower layers. These reflected waves have an additional impact on the mean flow in the MLT and even in the stratosphere.

The influence of SA at MLT heights can be seen in Fig. 4, which shows the latitude-altitude distributions of EP fluxes, temperature, RMC components and zonal wind at low SA for January, as well as changes in these parameters at high SA, similar to the data in Fig. 1, but for the altitude range of 75–115 km. A special feature is the downward EP flux southwards of 10° S, associated with an increase in the momentum flux $w'u'$ in Eq. (4) in this region. This is expressed in an increase in the speed of zonal and vertical winds, shown in Figs. 4c2 and 5b2, respectively. Bottom panels in Fig. 4 show that changes in SA above altitude of 100 km can lead to substantial changes in the temperature regime, RMC components and zonal circulation below level of 100 km. The magnitude of the RMC differences can reach 10% in the Northern Hemisphere. With increasing altitude, the area of significant RMC increments covers a larger latitudinal range. Above 95 km, statistically significant changes in the residual circulation cover both hemispheres. The area of maximum RMC and temperature increments approximately coincides with the waveguide structure for a stationary PW considered in Koval et al. (2019b), Fig. 3. This once again confirms the leading role of PWs in the formation of global atmospheric dynamics at the considered altitudes.

The effect of wave reflection is demonstrated by considering the Eliassen-Palm wave activity flux and changes in its structure due to changes in SA. Figure 4a2 shows that in the lower thermosphere the increments of EP fluxes are directed downward, which indicates a weakening of the upward propagation of wave activity and its reversal in this region at high SA. A similar scenario has been found previously, for example by Gan et al. (2017), who analyzed the EP flux in the stratosphere and discussed that under conditions of SA maximum, PW activity is weaker, which leads to the westerly zonal wind anomaly in the middle atmosphere.

To analyze wave impact on the RMC, we consider the terms on the right-hand side of Eqs. (1) and (2). Upper panels of Fig. 5 show the distributions of the RMC, the Eulerian mean circulation and the wave-induced eddy part of RMC for the altitude range of 75–115 km. It is shown in Fig. 5b1

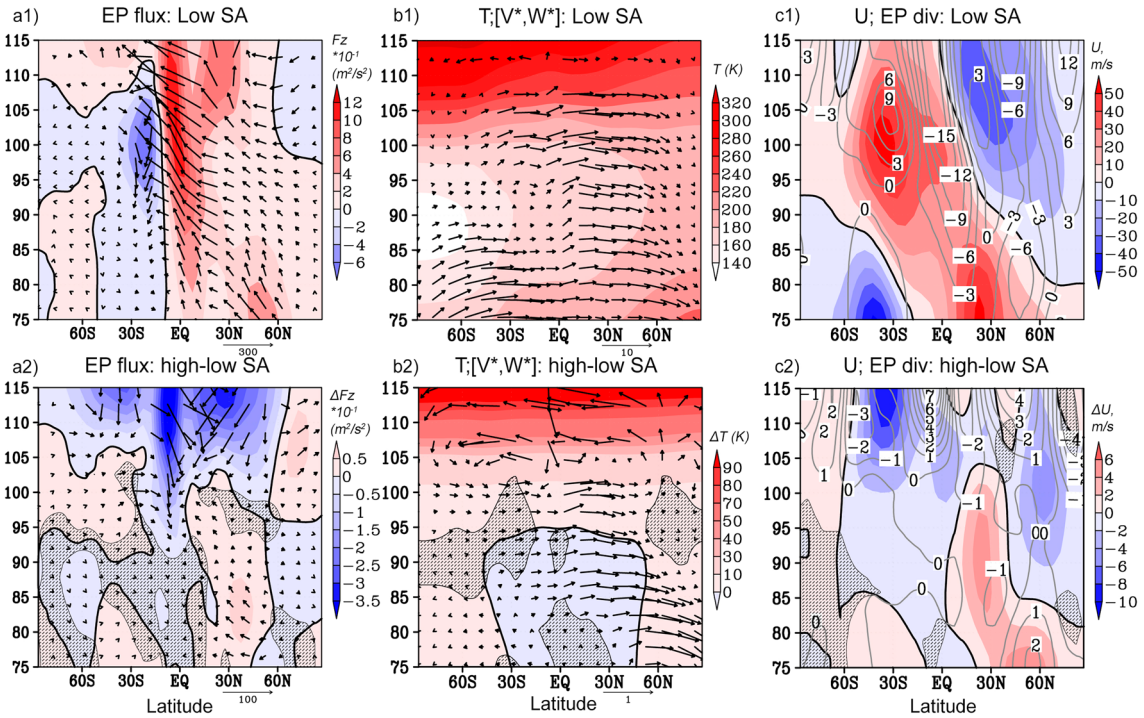

Fig. 4 Latitude-height distributions: **a**—EP flux (m^2/s^2, arrows) and its vertical component (color coded); **b**—zonal-mean temperature (K, color coded) and RMC (m/s, arrows); **c**—zonal-mean zonal wind (m/s, color coded) and EP flux divergence (10^2 m^2/s^2/day, contours). The top row corresponds to low SA, the bottom row presents the increments in the indicated parameters between high and low SA. The vertical RMC and EP flux components are multiplied by 200. Hatched areas indicate statistically insignificant data ($F^{(\varphi)}$ and $F^{(z)}$ components for (**a**); V^*, W^* and T increments for (**b**); U increment for (**c**))

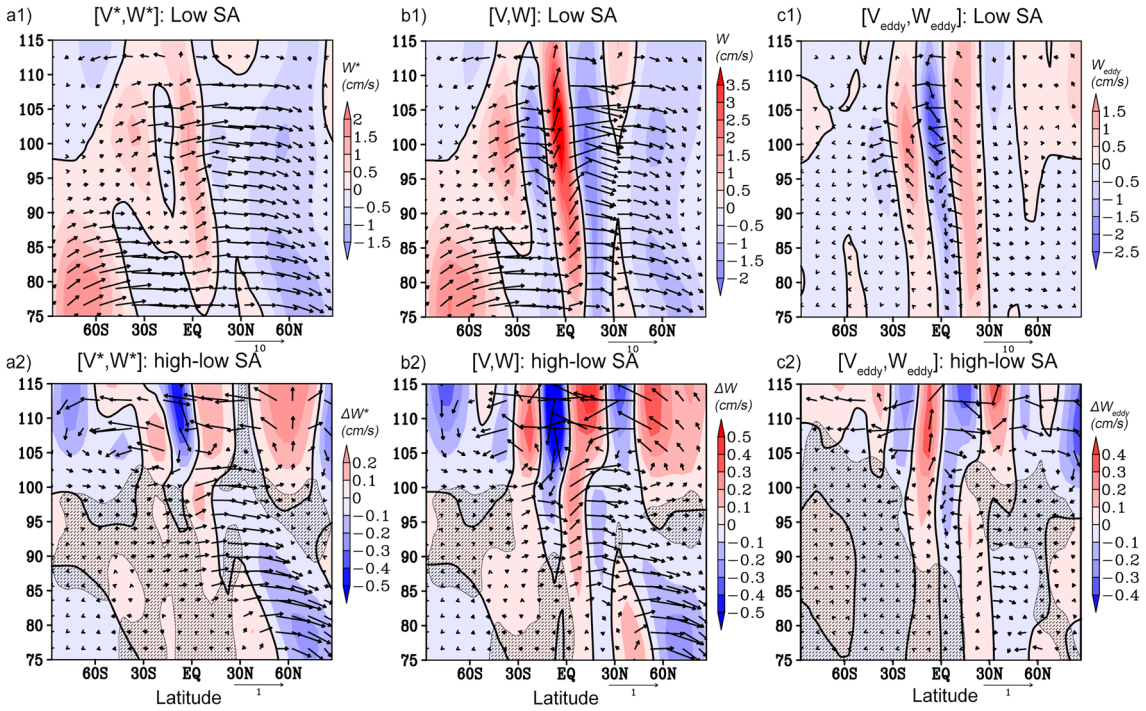

Fig. 5 Latitude-height distributions: RMC (**a**, repeating arrows in Fig. 4a), Eulerian mean circulation (**b**) and eddy component of the RMC (**c**) at low SA (upper row) and corresponding increments (bottom row). The vertical components are multiplied by 200. Color coded areas indicate statistically insignificant data

and c1, that the vertical part of the meridional circulation in the low-latitude region changes its direction with latitude, these components partially compensate each other (Fig. 5b1 and c1), which collectively leads to areas of upward circulation in the southern tropics and downward ones in the northern tropics (Fig. 5a1). A similar vertical flow structure was demonstrated at 90 km altitude by Teng et al. (2021). As our analysis showed, this is explained by spatial variations of the meridional wind, which is associated with vertical motion through the continuity equation, and apparently associated with the dissipation of GWs. The GW dependence on SA in the thermosphere was shown e.g., by Yiğit and Medvedev (2010), Klausner et al. (2009). In particular, variations in temperature, density, and static stability of the atmosphere are dependent on SA (see also Vadas and Fritts 2006; Laskar et al. 2015). These parameters impact the conditions for the GW propagation. The influence of GW is specified in MUAM using a number of parameterizations, but their effects are not analyzed using the TEM methodology, as far as these waves are unresolved on the MUAM spatial grid, and remain outside the scope of this study.

A remarkable feature of the EP flux distribution in Fig. 4a2 is strong upward wave activity flux in the layer of 80–100 km, in the latitude range of 10°–50° N. This enhancement, which can reach up to 25%, contributes to the strengthening of the eddy part of the RMC in this region (Fig. 5c2). It can be assumed that this enhancement is associated with the cumulative effect of upward propagating and reflecting PWs. It can be seen in Fig. 5c2 that the increments of the eddy circulation components in this region represent an additional contribution to the enhancement of RMC at high SA. The intensification of the meridional transfer of cold air masses from the summer mesopause to the winter hemisphere, determined mainly by the mean Eulerian circulation in Fig. 5b2, causes cooling of the low- and mid-latitude mesosphere. Further, winter high-latitude mesosphere, on the contrary, warms up due to adiabatic heating caused by the acceleration of the descending branch of the RMC.

Acceleration of the meridional RMC component in the Northern Hemisphere, at the layers between 70 and 100 km, presented in Fig. 4b2, according to the equation of motion, causes additional eastward-directed increments of the zonal flow shown in Fig. 4c2. This leads to an acceleration of the zonal wind speed in the specified region, except for the subpolar region above 80 km. Another reason of zonal wind intensification in the northern MLT is momentum deposition from the PW to the mean flow, expressed in increase in the EP flux divergence shown in Fig. 4c2 with contours. In general, similar tendencies in zonal wind and temperature in January were discussed by Karlsson and Kuilman (2018) based on numerical simulations using the CMAM model. Hence, our simulations show how changes in thermospheric

thermodynamic regime associated with solar cyclicity produce effects in the MLT area comparable in magnitude to direct impact of changes in solar radiation.

In this work we limited ourselves to a height of 75 ka and did not consider the effects of reflected PWs below this level. In lower layers, many mechanisms appear that are not related to the effect of solar activity changes under consideration. The changes that occur there depend significantly, for example, on the phases of the quasi-biennial oscillations, on the formation of sudden stratospheric warmings that may camouflage the effect of solar activity.

4 Conclusions

The study is devoted to investigation of the fundamental patterns of the influence of SA variations on changes in the dynamic and temperature regime of the thermosphere and the MLT area. Using the numerical mechanistic nonlinear Middle and Upper Atmosphere Model "MUAM", two 16-member ensembles of hydrodynamic fields under conditions of high and low SA were obtained. We concentrated on the influence of changes in SA that occurred only in the thermosphere, including the study of the transfer of this effect to the underlying layers. Therefore, in the numerical schemes of the MUAM, different levels of SA were specified in atmospheric layers above 100 km. The response of the dynamics of the MLT region and thermosphere on the changes in SA was considered from the point of view of the interaction of atmospheric circulation with PWs and tides. This interaction was analyzed using the TEM approach and interpreted by calculating the Eliassen-Palm flux and the residual meridional circulation (RMC).

With increasing solar influence at high SA, in the altitude range between 100 and 170 km, wave activity decreases. A number of factors contribute to this, including increased viscosity and vertical temperature gradients at high SA. The upward propagation of wave activity at high SA is weakened or even turns downward, creating conditions favorable for the reflection of PWs. Such reflected waves have an additional influence on the dynamics of the underlying layers. Above the level of 160–180 km, a wave activity strengthening is observed. To explain the multidirectional behavior of EP fluxes, changes in the amplitudes and EP fluxes of migrating solar diurnal and semidiurnal tides and stationary PWs with wavenumbers 1 and 2 were studied. According to the formulas for calculating the EP flux components, its magnitude is determined by temperature and velocity disturbances resolved on the MUAM model grid: planetary waves and tides. It was shown that the dominant role in the change of wave activity in the thermosphere at high SA is played by tides, the wave activity of which is mainly weakened below 160–180 km and strengthened above. The amplitudes of the PWs have significantly smaller values, as well as the EP fluxes.

Analysis of changes in the RMC in the thermosphere with increasing SA shows that the strengthening of the meridional component of the RMC above 200 km is determined by changes in the Eulerian mean circulation, the reason for which is the strengthening of the direct effect of the EUV irradiation and consequently, increased meridional pressure gradient. The contribution of SA to the change in the vertical RMC component at altitudes above 200 km is determined mainly by the eddy component: ascending eddy flows are localized in the latitudinal belt between 30º S and 30º N, along the trajectory of the diurnal thermal tide, and are compensated by downward flows in the subpolar and middle latitudes. Overall, this creates a complex, wave-like picture of the RMC changes in the thermosphere.

Changes in SA in the upper atmosphere (namely, they are set in the MUAM at altitudes of more than 100 km) induce substantial changes in the temperature regime and wind speed in the underlying layers. The magnitude of the RMC differences, for example, can reach 10% in the northern MLT area. The main role in these changes is played by the reflection of PWs at the lower thermosphere, which intensifies at high SA due to growing temperature gradients. This is evidenced by both the localization of changes in temperature and RMC along the PW propagation trajectory, as well as correspondingly directed EP fluxes. The PW reflection appears to be the cause of increased wave activity in the northern MLT area, which contributes to the RMC strengthening at high SA. This observed strengthening of the RMC at the MLT heights, as well as the moment transfer from PWs to the mean flow, in turn, contributes to the strengthening of the zonal circulation.

The significant increments in the temperature and mean zonal/meridional wind obtained below 100 km altitude confirm that alterations in thermospheric thermal and dynamic state caused by the SA influence can impact circulation in the MLT area, while PWs provide an effective mechanism for such vertical interaction. The idealized experiments, which isolate only one aspect in the formation of the overall forcing on the atmosphere, allows us to advance in understanding the nuances of large-scale atmospheric dynamics.

Author contributions All authors made valuable contributions to data analysis, visualization of the results, writing and editing the text. Andrey V. Koval: conceptualization, numerical modeling; Nikolai M. Gavrilov: consulting and proofreading; Kseniia A. Didenko: statistical processing; Tatiana S. Ermakova and Anastasiia G. Golovko: calculations within TEM framework.

Funding This work was supported by the Russian Science Foundation (grant #23-77-01035).

Data availability All rights to the MUAM computer code belong to the Russian State Hydrometeorological University (RSHU) in accordance with the statement 1296 of the Civil Code of the Russian Federation. To gain access to computer codes and acquire the right to use them, the reader must obtain permission from the Rector of the RSHU at the address: 192007, St. Petersburg, Voronezhskaya st., 79, phone: 007 (812) 372-50-92. The authors are ready to provide the necessary assistance in obtaining the appropriate permission. All datasets presented in the article are archived in Zenodo (https://doi.org/https://doi.org/10.5281/zenodo.11544885). All graphs in this study were generated using the Grid Analysis and Display System (GrADS), a free software developed by NASA's Advanced Information Systems Research Program.

Declarations

Conflict of interest The authors declare no competing interests.

References

Andrews DG, McIntyre ME (1976) Planetary waves in horizontal and vertical shear: the generalized Eliassen-Palm relation and the mean zonal acceleration. J Atmos Sci 33:2031–2048. https://doi.org/10.1175/1520-0469(1976)033%3c2031:PWIHAV%3e2.0.CO;2

Andrews DG, Holton JR, Leovy CB (1987) Middle atmosphere dynamics. Academic Press, New York

Arnold NF, Robinson TR (1998) Solar cycle changes to planetary wave propagation and their influence on the middle atmosphere circulation. Ann Geophys 16(1):69–76. https://doi.org/10.1007/s00585-997-0069-3

Arnold NF, Robinson TR (2000) Amplification of the influence of solar flux variations on the winter stratosphere by planetary waves. Space Sci Rev 94:279–286. https://doi.org/10.1023/A:1026783609783

Bal S, Schimanke S, Spangehl T, Cubasch U (2018) Enhanced residual mean circulation during the evolution of split type sudden stratospheric warming in observations and model simulations. J Earth Syst Sci 127:68. https://doi.org/10.1007/s12040-018-0972-x

Balogh A, Hudson HS, Petrovay K, von Steiger R (2014) Introduction to the solar activity cycle: overview of causes and consequences. Space Sci Rev 186:1–15. https://doi.org/10.1007/s11214-014-0125-8

Brewer AW (1949) Evidence for a world circulation provided by measurements of helium and water vapour distribution in the stratosphere. Q J R Meteorol Soc 75:351–363. https://doi.org/10.1002/qj.49707532603

Butchart N (2014) The Brewer-Dobson circulation. Rev Geophys 52:157–184. https://doi.org/10.1002/2013RG000448

Cai Q, Chen W, Chen S, Ma T, Garfinkel CI (2022) Influence of the Quasi-Biennial Oscillation on the spatial structure of the wintertime Arctic oscillation. J Geophys Res: Atmos 127, e2021JD035564. https://doi.org/10.1029/2021JD035564

Didenko KA, Koval AV, Ermakova TS, Sokolov AV, Toptunova ON (2024) Analysis of a secondary 16-day planetary wave generation through nonlinear interactions in the atmosphere. Earth Planets Space 76:124. https://doi.org/10.1186/s40623-024-02072-x

Dobson GMB (1956) Origin and distribution of polyatomic molecules in the atmosphere. Proc R Soc A236:187–193. https://doi.org/10.1098/rspa.1956.0127

Eyring V, Harris NRP, Rex M, Shepherd TG, Fahey DW, Amanatidis GT, Austin J, Chipperfield MP et al (2005) A Strategy for process-oriented validation of coupled chemistry-climate models. Bull Am Meteorol Soc 86:1117–1133. https://doi.org/10.1175/BAMS-86-8-1117

Fishman J, Crutzen PJ (1978) The origin of ozone in the troposphere. Nature 274:855–857. https://doi.org/10.1038/274855a0

Forbes JM, Zhang X, Ward W, Talaat ER (2002) Climatological features of mesosphere and lower thermosphere stationary planetary waves within ±40 latitude. J Geophys Res 107(D17):4322. https://doi.org/10.1029/2001JD001232

Forbes JM, Zhang X, Maute A, Hagan ME (2018) Zonally symmetric oscillations of the thermosphere at planetary wave periods. J Geophys Res: Space Phys 123:4110–4128. https://doi.org/10.1002/2018JA025258

Forbes JM, Zhang X, Maute A (2020) Planetary wave (PW) generation in the thermosphere driven by the PW-modulated tidal spectrum. J Geophys Res: Space Phys 125, e2019JA027704. https://doi.org/10.1029/2019JA027704

Fuller-Rowell TJ (1998) The "thermospheric spoon": a mechanism for the semiannual density variation. J Geophys Res 103(A3):3951–3956. https://doi.org/10.1029/97JA03335

Gan Q, Du J, Fomichev VI, Ward WE, Beagley SR, Zhang S, Yue J (2017) Temperature responses to the 11 year solar cycle in the mesosphere from the 31year (1979–2010) extended Canadian Middle Atmosphere Model simulations and a comparison with the 14year (2002–2015) TIMED/SABER observations. J Geophys Res: Space Phys 122(4):4801–4818. https://doi.org/10.1002/2016JA023564

Gavrilov NM, Koval AV (2013) Parameterization of mesoscale stationary orographic wave forcing for use in numerical models of atmospheric dynamics. Izv Atmos Ocean Phys 49(3):244–251. https://doi.org/10.1134/S0001433813030067

Geißler Ch, Jacobi Ch, Lilienthal F (2020) Forcing mechanisms of the migrating quarterdiurnal tide. Ann Geophys 38:527–544. https://doi.org/10.5194/angeo-38-527-2020

Geller MA, Alpert JC (1980) Planetary wave coupling between the troposphere and the middle atmosphere as a possible Sun-weather mechanism. J Atmos Sci 37:1197–1215. https://doi.org/10.1175/1520-0469(1980)037%3c1197:PWCBTT%3e2.0.CO;2

Gerber EP, Butler A, Calvo N, Charlton-Perez A, Giorgetta M, Manzini E et al (2012) Assessing and understanding the impact of stratospheric dynamics and variability on the earth system. Bull Am Meteorol Soc 93:845–859. https://doi.org/10.1175/BAMS-D-11-00145.1

Gulyaeva TL, Huang X, Reinisch BW (2002) Ionosphere-plasmasphere model software for ISO. Acta Geodaet Geophys Hungarica 37(2–3):143–152. https://doi.org/10.1556/AGeod.37.2002.2-3.3

Haynes PH, McIntyre ME, Shepherd TG, Marks CJ, Shine KP (1991) On the "downward control" of extratropical diabatic circulations by eddy-induced mean zonal forces. J Atmos Sci 48(4):651–678. https://doi.org/10.1175/1520-0469(1991)048%3c0651:OTCOED%3e2.0.CO;2

Holton JR (2004) An introduction to dynamic meteorology, fourth edition. Elsevier Academic Press, New York

Holton JR, Mass C (1976) Stratospheric vacillation cycles. J Atmos Sci 33, 2. https://doi.org/10.1175/1520-0469(1976)033<2218:SVC>2.0.CO;2

Holton JR, Haynes PH, McIntyre ME, Douglas AR, Rood RB, Pfister L (1995) Stratosphere-troposphere exchange. Rev Geophys 33:403–439. https://doi.org/10.1029/95RG02097

Jucker M (2021) Scaling of Eliassen-Palm flux vectors. Atmos Sci Lett 22(4):e1020. https://doi.org/10.1002/asl.1020

Karlsson B, Kuilman M (2018) On how the middle atmospheric residual circulation responds to the solar cycle close to the solstices. J Clim 31:401–421. https://doi.org/10.1175/JCLI-D-17-0202.1

Klausner V, Fagundes PR, Sahai Y, Wrasse CM, Pillat VG, Becker-Guedes F (2009) Observations of GW/TID oscillations in the F2 layer at low latitude during high and low solar activity,

geomagnetic quiet and disturbed periods. J Geophys Res 114, A02313. https://doi.org/10.1029/2008JA013448

Klimenko MV, Klimenko VV, Bessarab FS, Sukhodolov TV, Vasilev PA, Karpov IV, Korenkov YN, Zakharenkova IE, Funke B, Rozanov EV (2019) Identification of the mechanisms responsible for anomalies in the tropical lower thermosphere/ionosphere caused by the January 2009 sudden stratospheric warming. J Space Weather Space Clim 9, A39. https://doi.org/10.1051/swsc/2019037

Kobayashi S, Ota Y, Harada H (2015) The JRA-55 reanalysis: general specifications and basic characteristics. J Meteorol Soc Jpn 93:5–48. https://doi.org/10.2151/jmsj.2015-001

Kodera K, Kuroda Y (2002) Dynamical response to the solar cycle. J Geophys Res 107(D24):4749. https://doi.org/10.1029/2002JD002224

Kodera K, Mukougawa H, Itoh S (2008) Tropospheric impact of reflected planetary waves from the stratosphere. Geophys Res Lett 35, L16806. https://doi.org/10.1029/2008GL034575

Koval AV, Gavrilov NM, Pogoreltsev AI, Shevchuk NO (2018a) Influence of solar activity on penetration of traveling planetary-scale waves from the troposphere into the thermosphere. J Geophys Res: Space Phys 123(8):6888–6903. https://doi.org/10.1029/2018JA025680

Koval AV, Gavrilov NM, Pogoreltsev AI, Shevchuk NO (2018b) Propagation of stationary planetary waves in the upper atmosphere under different solar activity. Geomagn Aeron 58(2), 281–289. https://doi.org/10.1134/S001679321802010X

Koval AV, Gavrilov NM, Pogoreltsev AI, Drobashevskaya EA (2019a) Numerical simulation of the mean meridional circulation in the middle atmosphere at different phases of stratospheric warmings and mountain wave scenarios. J Atmos Solar Terr Phys 183:11–18. https://doi.org/10.1016/j.jastp.2018.12.012

Koval AV, Gavrilov NM, Pogoreltsev AI, Shevchuk NO (2019b) Reactions of the middle atmosphere circulation and stationary planetary waves on the solar activity effects in the thermosphere. J Geophys Res: Space Phys 124:10645–10658. https://doi.org/10.1029/2019JA027392

Koval AV, Gavrilov NM, Didenko KA, Ermakova TS, Savenkova EN (2022a) Sensitivity of the 4–10-day planetary wave structures in the middle atmosphere to the solar activity effects in the thermosphere. Atmosphere 13(8):1325. https://doi.org/10.3390/atmos13081325

Koval AV, Gavrilov NM, Pogoreltsev AI, Kandieva KK (2022b) Dynamical impacts of stratospheric QBO on the global circulation up to the lower thermosphere. J Geophys Res Atmos 127, e2021JD036095. https://doi.org/10.1029/2021JD036095

Koval AV, Toptunova ON, Motsakov MA, Didenko KA, Ermakova TS, Gavrilov NM, Rozanov EV (2023) Numerical modelling of relative contribution of planetary waves to the atmospheric circulation. Atmos Chem Phys 23:4105–4114. https://doi.org/10.5194/acp-23-4105-2023

Krivolutsky AA, Cherepanova LA, Dement'eva AV (2015) Solar cycle influence on troposphere and middle atmosphere via ozone layer in the presence of planetary waves: simulation with ARM. J Geophys Res Space Phys 120:8298–8306. https://doi.org/10.1002/2015JA021363

Kuroda Y, Makoto Deushi M, Shibata K (2007) Role of solar activity in the troposphere-stratosphere coupling in the Southern Hemisphere winter. Geophys Res Lett 34, L21704. https://doi.org/10.1029/2007GL030983

Labitzke K (1987) Sunspots, the Qbo, and the stratospheric temperature in the north polar-region. Geophys Res Lett 14(5):535–537. https://doi.org/10.1029/GL014i005p00535

Laskar FI, Pallamraju D, Veenadhari B, Lakshmi TV, Anji Reddy M, Chakrabarti S (2015) Gravity waves in the thermosphere: solar activity dependence. Adv Space Res 55(6):1651–1659. https://doi.org/10.1016/j.asr.2014.12.040

Laskar FI, McCormack JP, Chau JL, Pallamraju D, Hoffmann DP, Singh RP (2019) Interhemispheric meridional circulation during sudden stratospheric warming. J Geophys Res: Space Phys 124(8):7112–7122. https://doi.org/10.1029/2018JA026424

Laštovicka J (2006) Forcing of the ionosphere by waves from below. J Atmos Sol-Terr Phys 68(3):479–497. https://doi.org/10.5194/10.1016/j.jastp.2005.01.018

Lilienthal F, Jacobi C, Geißler C (2018) Forcing mechanisms of the terdiurnal tide. Atmos Chem Phys 18:15725–15742. https://doi.org/10.5194/acp-18-15725-2018

Lilienthal F, Yiğit E, Samtleben N, Jacobi C (2020) Variability of gravity wave effects on the zonal mean circulation and migrating terdiurnal tide as studied with the middle and upper atmosphere model (MUAM2019) using a nonlinear gravity wave scheme. Front Astron Space Sci 7:588956. https://doi.org/10.3389/fspas.2020.588956

Lindzen RS (1981) Turbulence and stress owing to gravity wave and tidal breakdown. J Geophys Res 86:9707–9714. https://doi.org/10.1029/JC086iC10p09707

Liu H-L (2016) Variability and predictability of the space environment as related to lower atmosphere forcing. Space Weather 14(9):634–658. https://doi.org/10.1002/2016SW001450

Liu HL, Richmond AD (2013) Attribution of ionospheric vertical plasma drift perturbations to large-scale waves and the difference on solar activity. J Geophys Res: Space Phys 2013, 108. https://doi.org/10.1002/jgra.50265

Lu H, Scaife AA, Marshall GJ, Turner J, Gray LJ (2017) Downward wave reflection as a mechanism for the stratosphere-troposphere response to the 11-year solar cycle. J Clim 30(N), 2395−2414. https://doi.org/10.1175/JCLI-D-16-0400.1

Mandal S, Pallamraju D, Suryawanshi P (2020) Changes in the daytime thermospheric gravity wave propagation characteristics over low-latitudes in response to the variation in solar flux. J Atmos Sol-Terr Phys 209:105414. https://doi.org/10.1016/j.jastp.2020.105414

Mukhtarov P, Pancheva D, Andonov B (2010) Climatology of the stationary planetary waves seen in the SABER/TIMED temperatures (2002–2007). J Geophys Res 115, A06315. https://doi.org/10.1029/2009JA015156.

Naito Y, Hirota I (1997) Interannual variability of the northern winter stratospheric circulation related to the QBO and the solar cycle. J Meteor Soc Jpn 75(4):925–937. https://doi.org/10.2151/jmsj1965.75.4_925

Nath D, Chen W, Lin W, Yin M (2014) Planetary wave reflection and its impact on tropospheric cold Weather over Asia during January 2008. Adv Atmos Sci 31:851–862. https://doi.org/10.2151/10.1007/s00376-013-3195-8

Oberheide J, Shiokawa K, Gurubaran S, Ward WE, Fujiwara H, Kosch MJ, Makela JJ, Takahashi H (2015) The geospace response to variable inputs from the lower atmosphere: a review of the progress made by Task Group 4 of CAWSES-II. Prog Earth Planet Sci 2(1):2. https://doi.org/10.1186/s40645-014-0031-4

Perlwitz J, Harnik N (2004) Downward coupling between the stratosphere and troposphere: the relative roles of wave and zonal mean processes. J Clim 17:4902–4909. https://doi.org/10.1175/JCLI-3247.1

Picone JM, Hedin AE, Drob DP, Aikin AC (2002) NRLMSISE-00 empirical model of the atmosphere: statistical comparisons and scientific issues. J Geophys Res Space Phys 107(A12):1468. https://doi.org/10.1029/2002JA009430

Pogoreltsev AI (2007) Generation of normal atmospheric modes by stratospheric vacillations. Izvestiya Atmos Ocean Phys 43(4):423–435

Pogoreltsev AI, Vlasov AA, Fröhlich K, Jacobi Ch (2007) Planetary waves in coupling the lower and upper atmosphere. J Atmos Solar-Terr Phys 69:2083–2101. https://doi.org/10.1016/j.jastp.2007.05.014

Qian L, Burns A, Yue J (2017) Evidence of the lower thermospheric winter-to summer circulation from SABER CO2 observations. Geophys Res Lett 44:10100–10107. https://doi.org/10.1002/2017GL075643

Richards PG, Fennelly JA, Torr DG (1994) EUVAC: a solar EUV flux model for calculations. J Geophys Res 99(A5):8981–8992. https://doi.org/10.1029/94JA00518

Shepherd TG (2007) Transport in the middle atmosphere. J Meteor Soc Jpn 85B:165–191. https://doi.org/10.2151/jmsj.85B.165

Sun R, Gu S, Dou X, Li N (2022) Tidal structures in the mesosphere and lower thermosphere and their solar cycle variations. Atmosphere 13(12):2036. https://doi.org/10.3390/atmos13122036

Swarztrauber PN, Kasahara A (1985) The vector harmonic analysis of Laplace's tidal equations. SIAM J Sci Stat Comp 6:464–491

Takahashi H, Wrasse CM, Fechine J et al (2007) Signatures of ultra fast Kelvin waves in the equatorial middle atmosphere and ionosphere. Geophys Res Lett 34, L11108. https://doi.org/10.1029/2007GL029612

Teng C-K-M, Gu S-Y, Qin Y, Dou X (2021) Impact of solar activity on global atmospheric circulation based on SD-WACCM-X simulations from 2002 to 2019. Atmosphere 12(11):1526. https://doi.org/10.3390/atmos12111526

Vadas SL, Fritts DC (2006) Influence of solar variability on gravity wave structure and dissipation in the thermosphere from tropospheric convection. J Geophys Res 111, A10S12. https://doi.org/10.1029/2005JA011510.

Vargin P, Kostrykin S, Koval A, Rozanov E, Egorova T, Smyshlyaev S, Tsvetkova N (2023) Arctic stratosphere changes in the 21st century in the Earth system model SOCOLv4. Front Earth Sci 11:1214418. https://doi.org/10.3389/feart.2023.1214418

Wang JC, Yue J, Wang W, Qian L, Wu Q, Wang N (2022) The lower thermospheric winter-to-summer meridional circulation: 1. Driving mechanism. J Geophys Res: Space Phys 127, e2022JA030948. https://doi.org/10.1029/2022JA030948

Ward W, Seppälä A, Yiğit E et al (2021) Role Of the Sun and the Middle atmosphere/thermosphere/ionosphere In Climate (ROSMIC): a retrospective and prospective view. Prog Earth Planet Sci 8:47. https://doi.org/10.1186/s40645-021-00433-8

Xiao C, Hu X, Tian J (2009) Global temperature stationary planetary waves extending from 20 to 120 km observed by TIMED/SABER. J Geophys Res 114, D17101. https://doi.org/10.1029/2008JD011349

Yamazaki Y, Richmond AD (2013) A theory of ionospheric response to upward-propagating tides: electrodynamic effects and tidal mixing effects. J Geophys Res: Space Phys 118:5891–5905. https://doi.org/10.1002/jgra.50487

Yiğit E, Medvedev AS (2009) Heating and cooling of the thermosphere by internal gravity waves. Geophys Res Lett 36, L14807. https://doi.org/10.1029/2009GL038507

Yiğit E, Medvedev AS (2010) Internal gravity waves in the thermosphere during low and high solar activity: simulation study. J Geophys Res 115, A00G02. https://doi.org/10.1029/2009JA015106.

Zorkaltseva OS, Mordvinov VI, Pogoreltsev AI, Dombrovskaya NS (2020) Dynamics of zonally averaged circulation characteristics in the middle atmosphere. Izvestiya Atmos Ocean Phys 56(4):378–389. https://doi.org/10.1134/S0001433820040118

Publisher's Note Springer Nature remains neutral with regard to jurisdictional claims in published maps and institutional affiliations.

Springer Nature or its licensor (e.g. a society or other partner) holds exclusive rights to this article under a publishing agreement with the author(s) or other rightsholder(s); author self-archiving of the accepted manuscript version of this article is solely governed by the terms of such publishing agreement and applicable law.